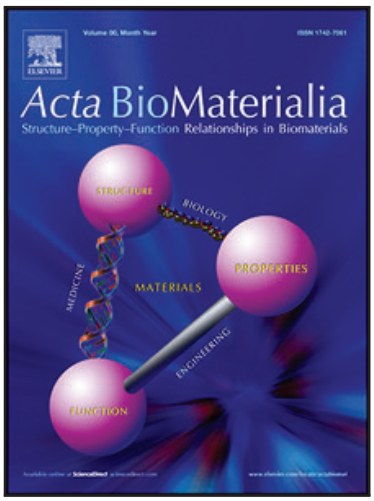

Elastic Fibers: The Missing Key to Improve Engineering Concepts for Reconstruction of the Nucleus Pulposus in the Intervertebral Disc

Javad Tavakoli , Ashish D. Diwan , Joanne L. Tipper

PII: S1742-7061(20)30329-9
DOI: https://doi.org/10.1016/j.actbio.2020.06.008
Reference: ACTBIO 6770

To appear in: *Acta Biomaterialia*

Received date: 12 April 2020
Revised date: 24 May 2020
Accepted date: 3 June 2020

Please cite this article as: Javad Tavakoli , Ashish D. Diwan , Joanne L. Tipper , Elastic Fibers: The Missing Key to Improve Engineering Concepts for Reconstruction of the Nucleus Pulposus in the Intervertebral Disc, *Acta Biomaterialia* (2020), doi: https://doi.org/10.1016/j.actbio.2020.06.008

Elastic Fibres: The Missing Key to Improve Engineering Concepts for Reconstruction of the Nucleus Pulposus in the Intervertebral Disc

Javad Tavakoli[1,2*], Ashish D. Diwan[1,2,3], Joanne L. Tipper[1*]

[1]Centre for Health Technologies, School of Biomedical Engineering, Faculty of Engineering and Information Technology, University of Technology Sydney, NSW, Australia

[2]SpineLabs, St George & Sutherland Clinical School, The University of New South Wales,

[3]Spine Service, Department of Orthopaedic Surgery, St George Hospital Campus, NSW, Australia

*Corresponding authors: Joanne L. Tipper (joanne.tipper@uts.edu.au), Javad Tavakoli (javad.tavakoli@uts.edu.au)

Abstract

The increasing prevalence of low back pain has imposed a heavy economic burden on global healthcare systems. Intense research activities have been performed for the regeneration of the Nucleus Pulposus (NP) of the IVD; however, tissue-engineered scaffolds have failed to capture the multi-scale structural hierarchy of the native tissue. The current study revealed for the first time, that elastic fibers form a network across the NP consisting of straight and thick parallel fibers that were interconnected by wavy fine fibers and strands. Both straight fibers and twisted strands were regularly merged or branched to form a fine elastic network across the NP. As a key structural feature, ultrathin (53 ± 7 nm), thin (215 ± 20 nm), and thick (890 ± 12 nm) elastic fibers were observed in the NP. While our quantitative analysis for measurement of the thickness of elastic fibers revealed no significant differences ($p < 0.633$), the preferential orientation of fibers was found to be significantly different ($p < 0.001$) across the NP. The distribution of orientation for the elastic fibers in the NP represented one major organized angle of orientation except for the central NP. We found that the distribution of elastic fibers in the central NP was different from those located in the peripheral regions

representing two symmetrically organized major peaks (±45º). No significant differences in the maximum fiber count at the major angles of orientation (±45º) were observed for both peripheral ($p = 0.427$) and central NP ($p = 0.788$). Based on these new findings a structural model for the elastic fibers in the NP was proposed. The geometrical presentation, along with the distribution of elastic fibers orientation, resulting from the present study identifies the ultrastructural organization of elastic fibers in the NP important towards understanding their mechanical role which is still under investigation. Given the results of this new geometrical analysis, more-accurate multiscale finite element models can now be developed, which will provide new insights into the mechanobiology of the IVD. In addition, the results of this study can potentially be used for the fabrication of bio-inspired tissue-engineered scaffolds and IVD models to truly capture the multi-scale structural hierarchy of IVDs.

Keywords

elastic fibers, ultrastructure, intervertebral disc, tissue engineering, nucleus pulposus

Statement of significance

Visualization of elastic fibers in the nucleus of the intervertebral disc under high magnification was not reported before. The present research utilized extracellular matrix partial digestion to address significant gaps in understanding of nucleus microstructure that can potentially be used for the fabrication of bio-inspired tissue-engineered scaffolds and disc models to truly capture the multi-scale structural hierarchy of discs.

1. Introduction

The intervertebral disc (IVD) is a three-component structure comprised of a central, gelatinous nucleus pulposus (NP) and surrounding annulus fibrosus (AF) situated between superior and inferior cartilaginous endplates that interface with the vertebral bodies. The AF is a multi-lamellar structure that is packed with well-organized collagen bundles forming a reinforcing structure. The NP is highly hydrated, rich in aggrecan and has a delicate collagen meshwork with no apparent organization [1].

The increasing prevalence of low back pain has imposed a heavy economic burden on global healthcare systems. Due to the limited availability and efficacy of direct treatment options, IVD structural defects often heal poorly and contribute to the initiation and progression of degeneration over time. While IVD degenerative changes and their association with low back pain are complex, studies have shown aging, genetic predeposition, occupation, and IVD disruption may lead to IVD degeneration causing low back pain [2, 3]. Treatments for IVD degeneration to stop or reverse this process are challenging since the IVD is the largest avascular structure in the body [4, 5]. IVD cells are also exposed to large magnitudes of loading during daily activities, exceeding more than 5-times body weight [6]. Furthermore, a lack of engineered tissues recapitulating the intrinsic complexity of the IVD structure is a severe limitation toward re-establishing function [7-9]. It is believed that the NP plays a major role in IVD degeneration by losing the capacity to bind water, leading to a significant reduction of IVD height under load, therefore intense research activities have been performed for the regeneration of the NP [10-12]. However, innovative injectable hydrogels that are currently used as tissue-engineered scaffolds for regeneration of the NP, despite encouraging laboratory and preclinical findings, do not restore native structures (at the micro and sub-micron level) and function, and therefore thay have not achieved prevalent clinical adoption

[13-15]. A suitable approach to identify the intrinsic complexity of the NP ultrastructure is essential for the construction of more clinically relevant tissue-engineered scaffolds to address a major gap for clinical translation [16]. To achieve this, new insights into the structural organization of elastic fibers within the NP is essential, since a large number of studies have focused on the structure and properties of only the collagen fibers in the NP.

The presence of elastic fibers, as a critical microstructural component, to control the elasticity of the IVD and withstand large deformation at changes has been explained in some number of previous studies [17-20]. Early anatomical studies based on light microscopic investigations, revealed an irregular distribution of elastic fibers across the NP [21-23]. Later, the observation of histologically-prepared samples under a conventional light microscope revealed that elastic fibers with 150 μm length were orientated radially in the NP [19, 20]. Unfortunately, traditional approaches for anatomical studies have failed to identify the ultrastructural organization of elastic fibers in the NP, since they are intermingled with other fibrous components and are mostly obscured by the extracellular matrix. The anatomical studies based on light microscopic analysis have not been able to reveal the fine-scale architectural details of the elastic fiber network.

Recently, a new research tool was developed for IVD anatomical studies, to eliminate all components except for elastic fibers utilizing sonication of tissue in sodium hydroxide solution (digestion technique) [24, 25]. It was confirmed that using this technique the *in situ* isolated elastic fibers remained chemically intact with minimal structural alteration. This resulted in new insights into the structure-function properties of elastic fibers in the AF of sheep IVD that were unattainable before [26-29]. It was identified that elastic fibers create an orthotropic network in both the inter-lamellar matrix and lamellae of the AF [30]. Within the elastic network, both thick and thin fibers are organized at ±45° with the majority (>70%) of them oriented at 0° [26, 30]. Also, it was found that the elastic network in the inter-lamellar

region of the AF is strain-rate dependent during dynamic loading, particularly for absorbed energy and stiffness and its failure strength is significantly higher in tension compared to the shear direction of loading [28, 29]. While these studies clarified a number of unknown characteristics of elastic fibers in the AF, the ultrastructural organization of elastic fibers in the NP is not known and whether they form a network across the NP is yet to be investigated. Therefore the aims of the current study were two-fold. Firstly, to determine the ultrastructural organization of elastic fibers across the NP in sheep IVD using Scanning Electron Microscopy and secondly to develop a structural model for the elastic fibers in the NP using quantitative analysis. The combination of this new knowledge will ultimately contribute to the development of more reliable tissue-engineered scaffolds for NP regeneration. The results of this study will help to understand the basic mechanical and biological role of elastic fibers in the NP, and more importantly, develop a platform for the fabrication of tissue-engineered scaffolds for repair, replacement, and regeneration of the NP.

Based on a previously published NaOH digestion technique [24], this study was performed on different regions of the NP (center, anterolateral and posterolateral regions in both right and left sides) to capture a comprehensive picture of the ultrastructural organization of elastic fibers throughout the NP. Isolated NPs from six lumbar sheep IVDs, located at level L4/L5, were utilized. A sheep model was used for the current study based on its structural, composition, appearance and aspect ratio, load profile and cell phenotype similarities to the human IVD.

2. Materials and methods

2.1. Sample preparation

Six fresh lumbar sheep spines (>18 months old) were obtained from a local abattoir. The IVDs (Figure 1a) from the L4/L5 level were carefully separated from the vertebrae and stored

at -20ºC for 24 h. While frozen, the entire NP was isolated from the peripheral AF for all IVDs using a surgical blade. From each NP (n = 6), five regions of interest were prepared. The central region (C) of the NP was separated using a sharp circular punch (hollow tip, diameter = 5 mm), and the remaining NP tissue was cut into four regions of posterolateral and anterolateral from both right and left sides (Figure 1b; LAL: left anterolateral; LPL: left posterolateral; RPL: right posterolateral and RAL: right anterolateral). Finally, two axial samples (thickness ≈ 1 mm) from each region were cut. A. One sample served as control and the other was digested for the ultrastructural study. To identify the lateral axis during image analysis, the cutting edge of samples was carefully marked with a mixture of superglue and ink after dissection.

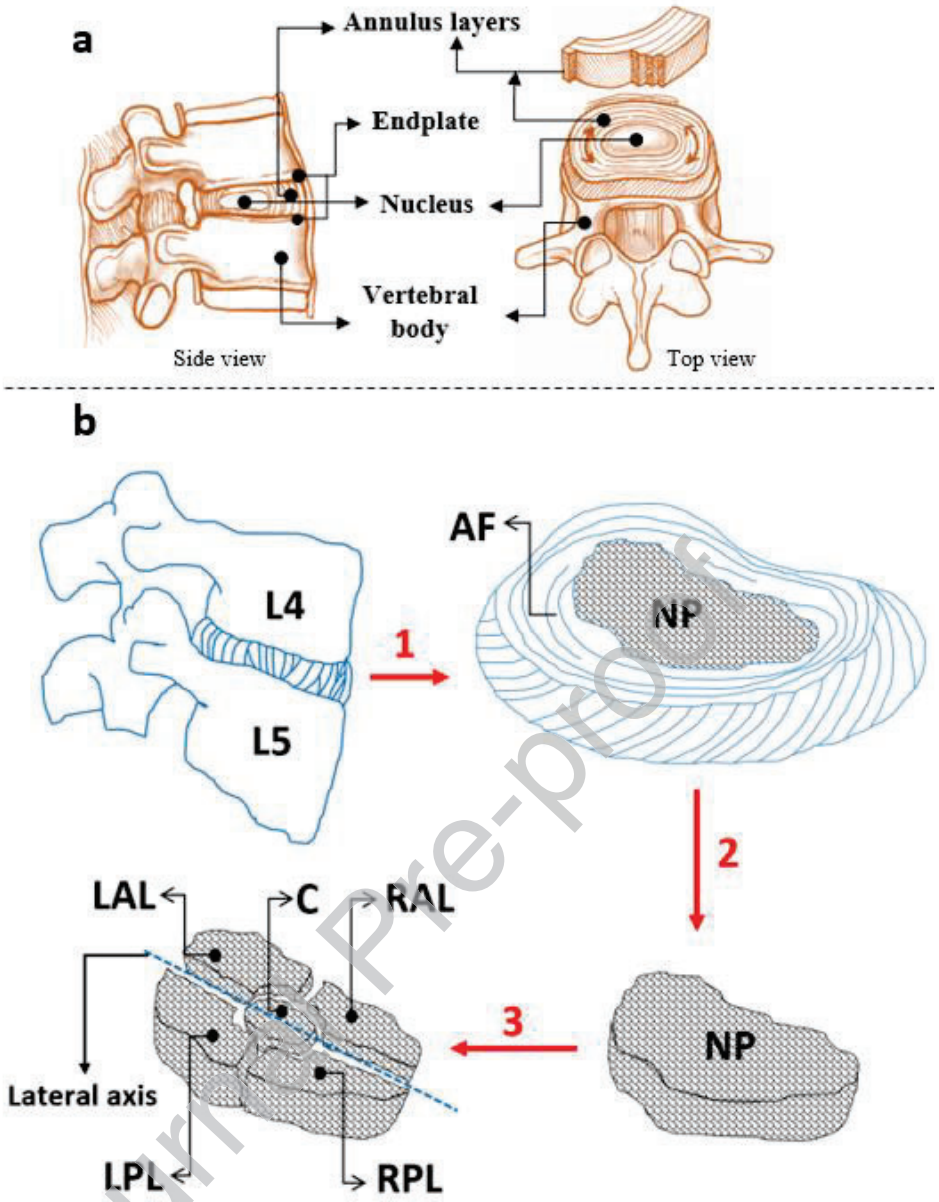

Figure 1- a) Main structural components of an IVD and b) Schematic drawing indicating sample preparation strategy (AF= Annulus Fibrosus, NP= Nucleus Pulposus, RAL= Right Anterolateral, RPL= Right Posterolateral, LPL= Left Posterolateral, LAL= Left Anterolateral, and C= Central). The red arrows represent the process that was performed to prepare the samples including (1) isolation of IVD from the adjacent bone, (2) separation of the NP from IVD and (3) dissection of NP to prepare the regions of interest. The lateral axis, denoted by the dotted blue line, was used for quantitative analysis to measure the orientation

of fibers after digestion. The lateral axis of the IVD was consistent among all samples during the experiments.

2.2. Sample digestion

To partially digest the sample, for *in situ* isolation of elastic fibers, the previously published method [24] was used with modifications. Briefly, samples were placed in NaOH (0.5 mM) solution, while being sonicated (950 W) for 30 min. After sonication, while still soaked in NaOH solution, samples were placed in an oven (T = 65º C) for 5-10 min. Then samples were washed gently using distilled water, dried in a series of graded ethanol (50 – 100% (step = 10%) for 5 min each), and finally were placed in a vacuum oven at 37ºC and -80 kPa for 1 h.

2.3. Scanning electron microscopy

All SEM images were captured from the surface of the samples after they were mounted on aluminum stubs using double adhesive tape. Before imaging, all samples were sputter-coated with platinum at 3 nm thickness. For SEM imaging the voltage was set to 5 kV and the distance from the surface of the sample to the beam source kept constant at 15 mm during imaging.

2.4. Quantitative analysis

For quantitive analysis, the thickness, preferential orientation, and distribution of orientation of elastic fibers in each region of interest were evaluated. SEM images were used for the measurement of the thickness of elastic fibers. The thickness of long and straight fibers was measured to represent thick elastic fibers. Also, the thicknesses of interconnecting wavy fibers and straight strands were measured to identify thin and ultrathin elastic fibers. The results for the fiber thickness were presented as the average of at least 3 measurements across all five regions of interest in all 6 samples.

Open source FIJI software was used to measure the preferential orientation and distribution of fiber orientation. SEM images were edited by selecting the automatic threshold with noise threshold, Lambda factor, and minimum leaf size equal to 25, 3, and 87, respectively. These threshold values were selected to edit SEM images to properly distinguish the elastic network from the background and were kept constant for all images during analysis (Segmentation plugin). Suggested by ImageJ software, the Cubic Spline was selected as it is fast, accurate, and quasi-isotropic with minimum boundary artifacts. Therefore, the Cubic Spline Gradient structural tensor with Gaussian window = 1 and minimum intensity = 50% was selected to measure the preferential orientation and distribution of fibers orientation.

The preferential orientation, representing the overall directionality of the fibers in each region, was measured using the OrientationJ plugin (Dominant Direction). All orientations were measured relative to the lateral axis of the IVD, which was kept consistent among all samples during the experiment, as shown in Figure 1. For measurement of the distribution of fibers orientation, edited SEM images served as the input (6 SEM images for each region of interest) using OrientationJ plugins (OrientationJ Distribution), and data were presented as an average of 6 measurements. Moreover, the OrientationJ plugin (DirectionJ analysis) was employed to create energy and color-survey (HSB) images to evaluate the current state, fiber detection accuracy and distribution of fiber orientation of edited images, respectively (Supplementary S1).

2.5. Statistical analysis

One way ANOVA was conducted (IBM SPSS Statistics for Windows, Version 26, Armonk, NY: IBM Corp.), having test variables of fiber orientation, thickness, and maximum fiber counts between different regions (C: center, LAL: left anterolateral; LPL: left posterolateral; RAL: right anterolateral; RPL: right posterolateral; and LA: lateral) using an alpha of 0.05.

Tukey post hoc was recruited when the assumption of homogeneity of variances was significant. While the assumption of the homogeneity of variances was violated, but the robust test of equality of means using Welch and Brown-Forysth analyses was significant, Games-Howell Post hoc was used.

3. Results

While the concentration of sodium hydroxide, thickness of samples and intensity of the ultrasound remained unchanged, the digestion process was optimized through the adjustment of sonication time. Since the fibrous constituents of the NP (collagen and elastic fibers) were obscured by the extracellular matrix, the observation of elastic fibers was impossible (Figure 2a) in the control (undigested) samples. Elimination of the extracellular matrix through a continuous mild sonication process (Figure 2b, 2c) revealed a progressive improvement in the visualization of elastic fibers in the NP (Figure 2d).

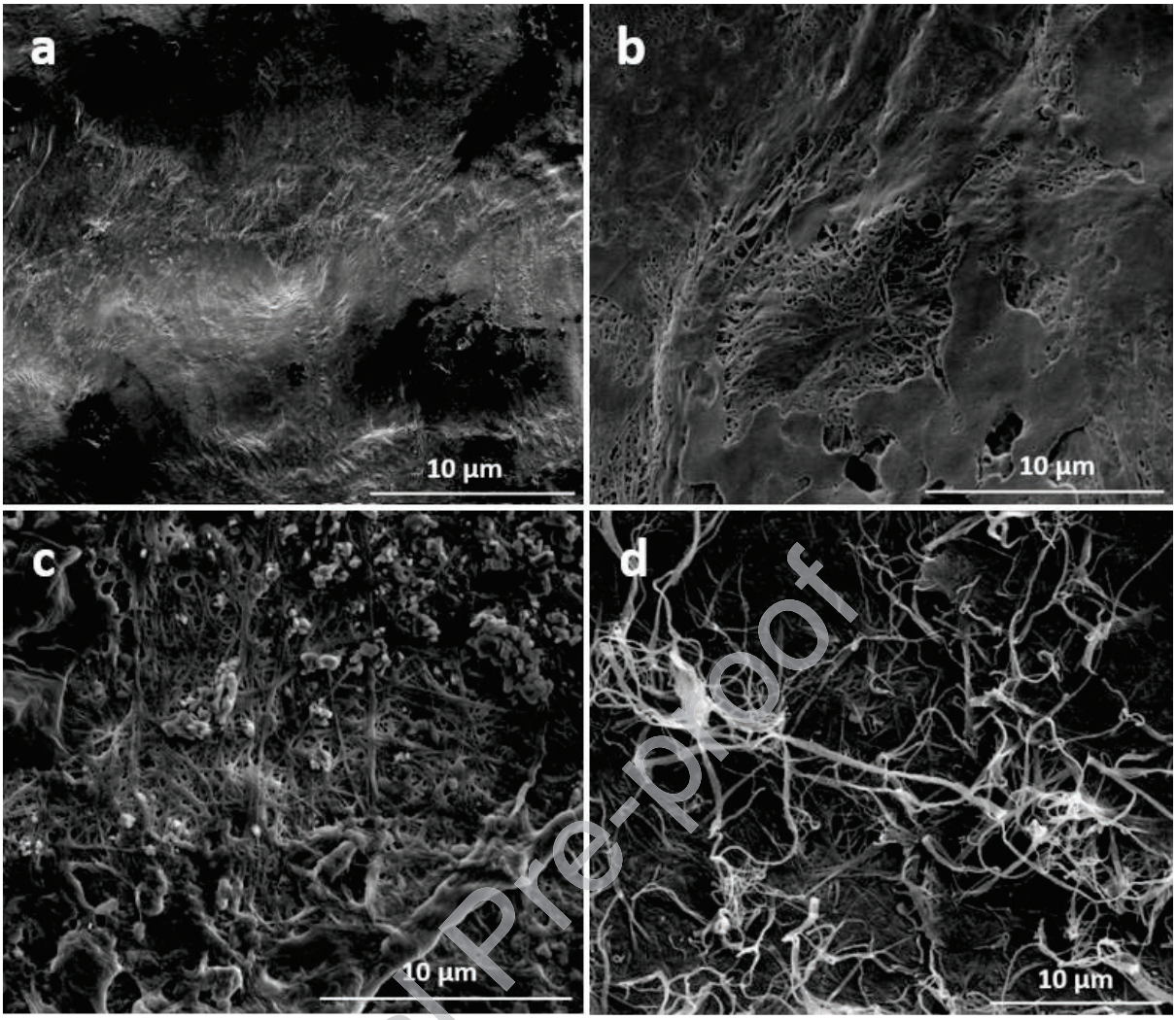

Figure 2- Optimization of the digestion process at different time points visualized by SEM imaging using the NP samples with 1 mm thickness including a) control (undigested) sample and b, c, d) digested samples after 10, 20 and 30 minutes sonication, respectively. The ultrastructure of elastic fibers appeared after approximately 30 minutes of sonication post-treatment.

The current study revealed for the first time, that elastic fibers form a network across the NP. It was found that the network of elastic fibers in the NP consists of straight and thick parallel fibers that were interconnected by wavy fine fibers and strands (Figure 3a). Both straight fibers and twisted strands were regularly merged or branched (denoted by arrows) to form a fine elastic network across the NP (Figure 3b). As a key structural feature among all digested

samples ultrathin (53 ± 7 nm), thin (215 ± 20 nm), and thick (890 ± 12 nm) elastic fibers were observed in the NP (Figure 3c). Based on the SEM images that were captured under lower magnifications (1000X- 2000X), long (> 250 μm) straight elastic fibers were also observed within the NP. The observation of the long fibers that are interlocked by fine wavy fibers (Figure 3d) clarifies that the concept of isolated elastic fibers in the NP, as previously reported through light microscopic investigations, was incorrect [21, 31]. Within the elastic fiber network, entangled nodes were observed in different regions. These high-density nodes, resembling the physical crosslinking regions of hydrogels, are likely to have an impact on the viscoelastic properties of the NP (Figures 3e, 3f). Figure 4 shows the frequently occurring structural features, the existence of a complex network comprising interconnected thin and thick elastic fibers, for all regions of interest (RAL, LAL, LPL, RPL, and C) across three samples.

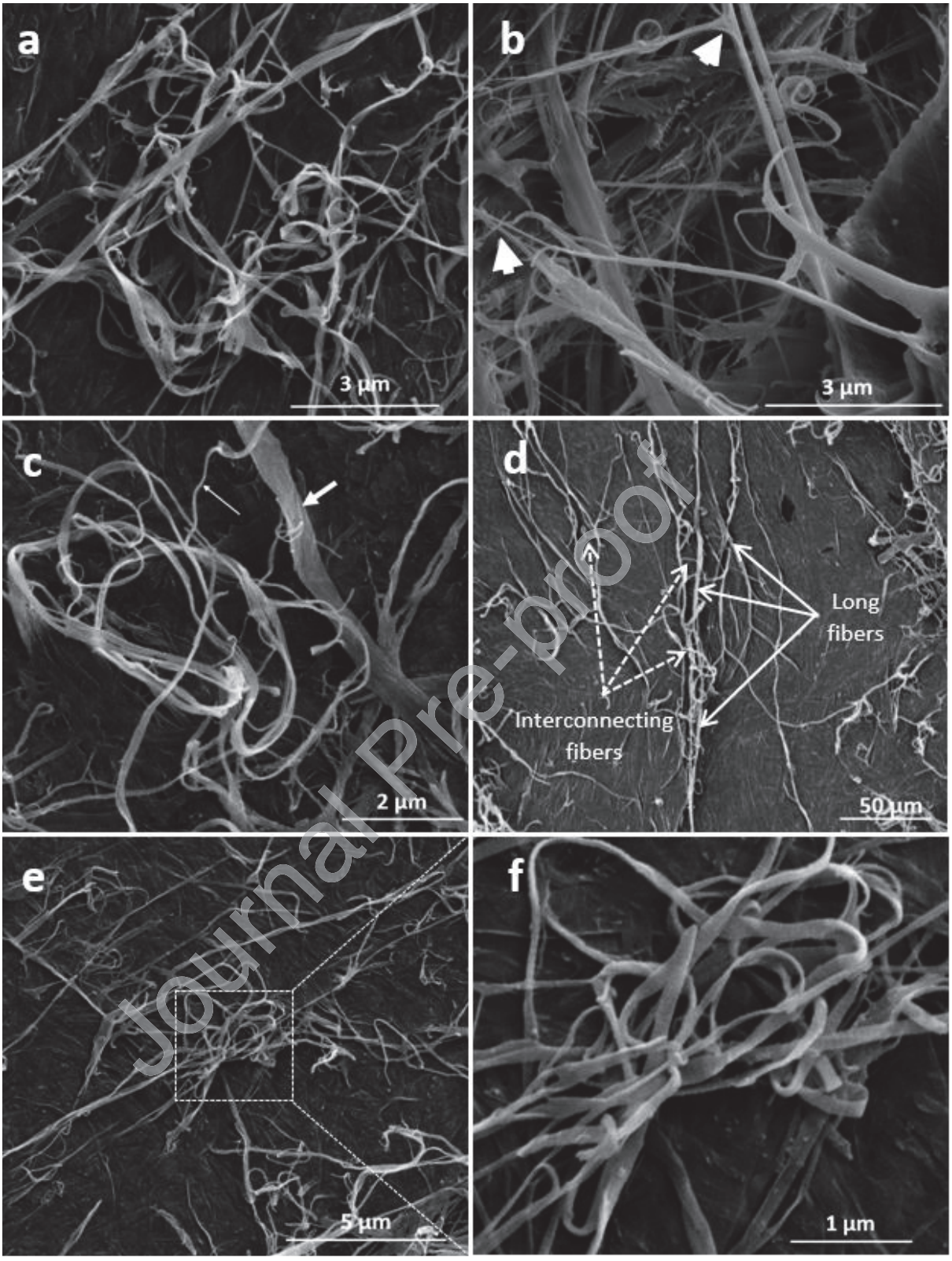

Figure 3- General observations for the ultrastructural organization of elastic fibers in the NP that was frequently seen among all samples in different regions of interest. a) Elastic fibers form a fine network across the NP. b) Key structural features, fibers branch (top arrowhead)

or merge (bottom arrowhead) regularly. c) Different shapes and sizes of fibers (denoted by white arrows), and d) long elastic fibers were observed within the elastic network. e, f) Entangled elastic fibers creating a high-density node viewed at two different magnifications for the same point.

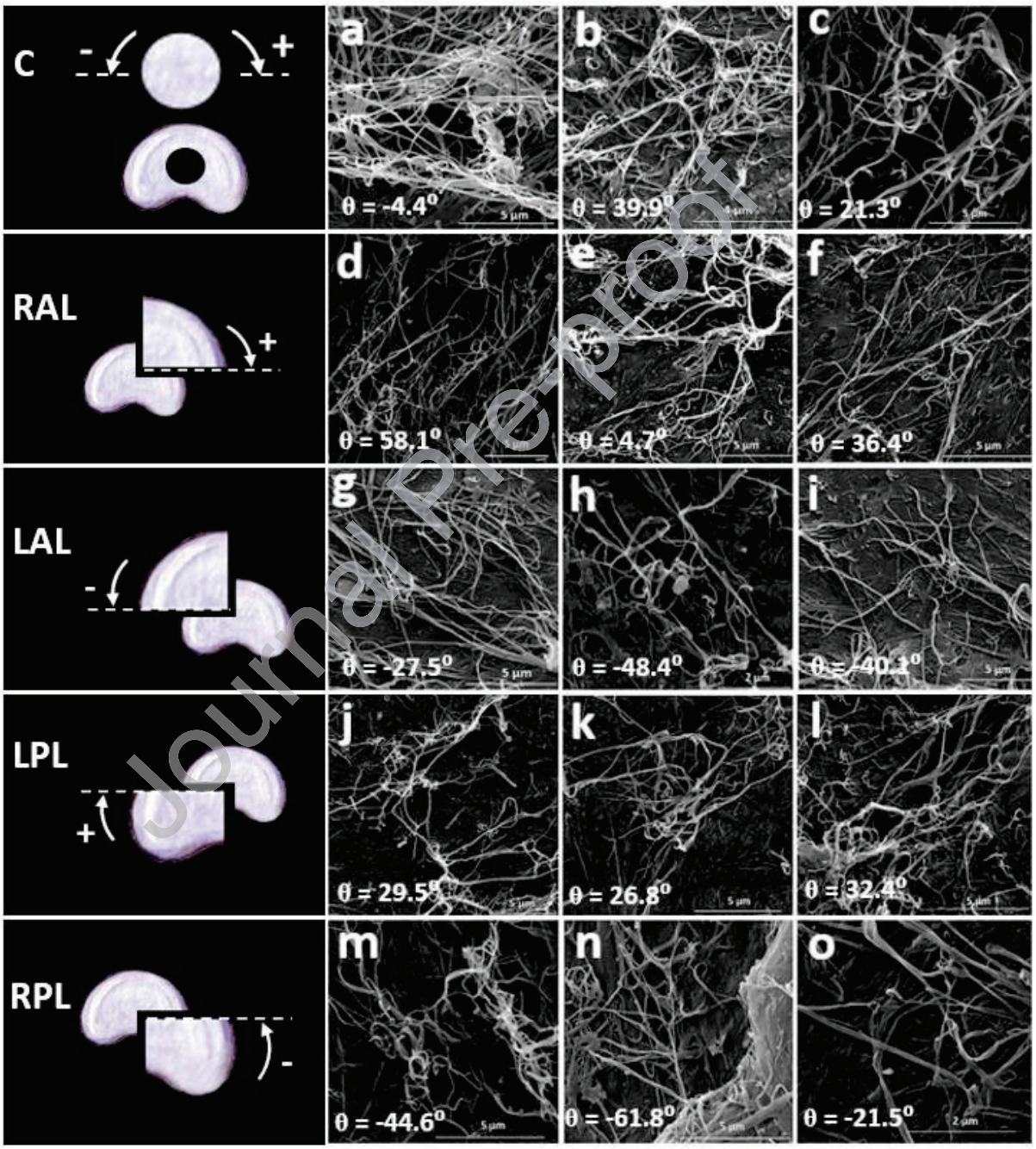

Figure 4 – Frequently occurring features of an elastic network in different regions of interest in the NP including (a-c) central (C), (d-f) right anterolateral (RAL); (g-h) left anterolateral (LAL), (j-l) left posterolateral (LPL), and (m-o) right posterolateral (RPL) across three different samples. θ represents the preferential orientation of elastic fibers and the orientation of fibers. Schematic drawings indicating the regions of interest with the preferential orientations of fibers (θ), measured relative to the lateral axis of the IVD (white dotted lines), denoted by white arrows.

Our quantitative analysis for measurement of the thickness of elastic fibers (Table 1) revealed no significant differences for the thickness of ultrathin ($p = 0.156$), thin ($p = 0.633$), and thick fibers ($p = 0.486$) across all regions of interest in the NP.

Table 1- Summary of the average fiber thickness for elastic fibers in different regions of the NP (LAL: left anterolateral; LPL: left posterolateral; RPL: right posterolateral; RAL: right anterolateral and C: center).

Region	Sample	Fiber thickness (µm)		
		ultrathin	thin	thick
C	1	0.07	0.26	0.81
	2	0.05	0.22	1.20
	3	0.06	0.19	0.80
	4	0.05	0.20	0.88
	5	0.05	0.23	0.82
	6	0.06	0.22	0.94
RAL	1	0.05	0.24	0.91
	2	0.05	0.23	0.95
	3	0.04	0.24	0.89
	4	0.04	0.02	0.90
	5	0.05	0.22	1.11
	6	0.05	0.21	0.97
LAL	1	0.06	0.21	0.86
	2	0.06	0.23	0.93
	3	0.06	0.19	0.86
	4	0.05	0.18	0.80
	5	0.05	0.21	0.92
	6	0.04	0.22	0.97
LPL	1	0.07	0.22	1.00
	2	0.06	0.19	0.84
	3	0.06	0.19	0.86
	4	0.05	0.22	1.09
	5	0.05	0.23	0.86
	6	0.05	0.24	0.94
RPL	1	0.06	0.19	0.95
	2	0.05	0.20	0.96
	3	0.04	0.23	0.98
	4	0.06	0.19	0.89
	5	0.05	0.23	0.88
	6	0.05	0.24	0.99
Mean(±Std)		**0.053 (0.007)**	**0.215 (0.02)**	**0.89 (0.012)**
P value		0.156	0.633	0.486

Quantitative analysis for measurement of the orientation of elastic fibers (Table 2), using FIJI software, revealed different angles of orientation were present in different regions of the NP.

Table 2- Summary of fiber orientation for elastic fibers in different regions of the NP (LAL: left anterolateral; LPL: left posterolateral; RPL: right posterolateral; RAL: right anterolateral and C: center). The fiber orientation was measured relative to the lateral axis of the IVD with clockwise (CW) and counter-clockwise (CCW) rotations being considered by + and – signs, respectively. The lateral axis of the IVD was consistent among all samples during the experiments.

Sample	**Regions**				
	LAL	LPL	RPL	RAL	C
Sample 1	-40.1	8.3	-61.8	58.1	-4.4
Sample 2	-15.6	26.8	-40.9	63.5	-13.8
Sample 3	-48.4	20.8	-44.6	36.4	-63.1
Sample 4	-27.5	29.5	-51.8	4.7	-29.6
Sample 5	-36.6	32.4	-71.5	51.4	21.3
Sample 6	-59.3	37.7	-21.5	11.9	39.9
Mean(±Std)	**-37.9(15.3)**	**25.9(10.3)**	**-48.7(17.4)**	**37.8(24.5)**	**-8.3(36.6)**
Antriolateral compared to Posterolateral:		**LAL- LPL**: $p < 0.001$, **RAL-RPL**: $p < 0.001$			
Left NP compared to the right NP:		**LAL-RAL**: $p = 0.001$, **LPL-RPL**: $p < 0.001$			

The average orientation of elastic fibers for the central NP (C) was close to zero (-8.3º). The large standard deviation of ±36.6º, along with observation of both clockwise (CW; +) and counter-clockwise (CCW; -) directions of rotation for elastic fibers indicated that the elastic fibers in this region were orientated in a wide range of angles (-63º to 40º). In contrast, the orientation of elastic fibers in other regions of the NP were either CW or CCW with lower standard deviations around the mean values. Statistical analysis showed that the overall preferential fiber orientation was significantly different amongst regions ($p < 0.001$). While the assumption of the homogeneity of variances has been violated ($p = 0.086$), it was found

that the robust test of equality of means for fiber orientation was significant using Welch and Brown-Forysth analyses ($p < 0.001$). Using Games-Howell as a post hoc test, it was found that the fiber orientation for the center was not significantly different from other regions of the NP ($p > 0.164$). The statistical analysis revealed that:

1- For both the left and right sides of the NP, the fiber orientation between the anterolateral and posterolateral regions of the NP was significantly different (between LAL - LPL, and between RAL - RPL; $p < 0.001$).
2- For both anterolateral and posterolateral regions, the orientation of fibers between the right and left side of the NP was significantly different (between LPL - RPL; $p < 0.001$ and between LAL - RAL; $p = 0.001$).

These findings were based on image analysis that was performed on the SEM images captured. It was observed that the orientation of elastic fibers in the center differs from those located in other regions of the NP (Figure 5). Even though, the key ultrastructural characteristics — the existence of a complex network comprising interconnected thin and thick elastic fibers — were almost similar amongst all regions. Apparently, in all regions of the NP except the central region, elastic fibers were extended from the center towards the AF, and therefore likely to provide a continuous elastic network across the IVD.

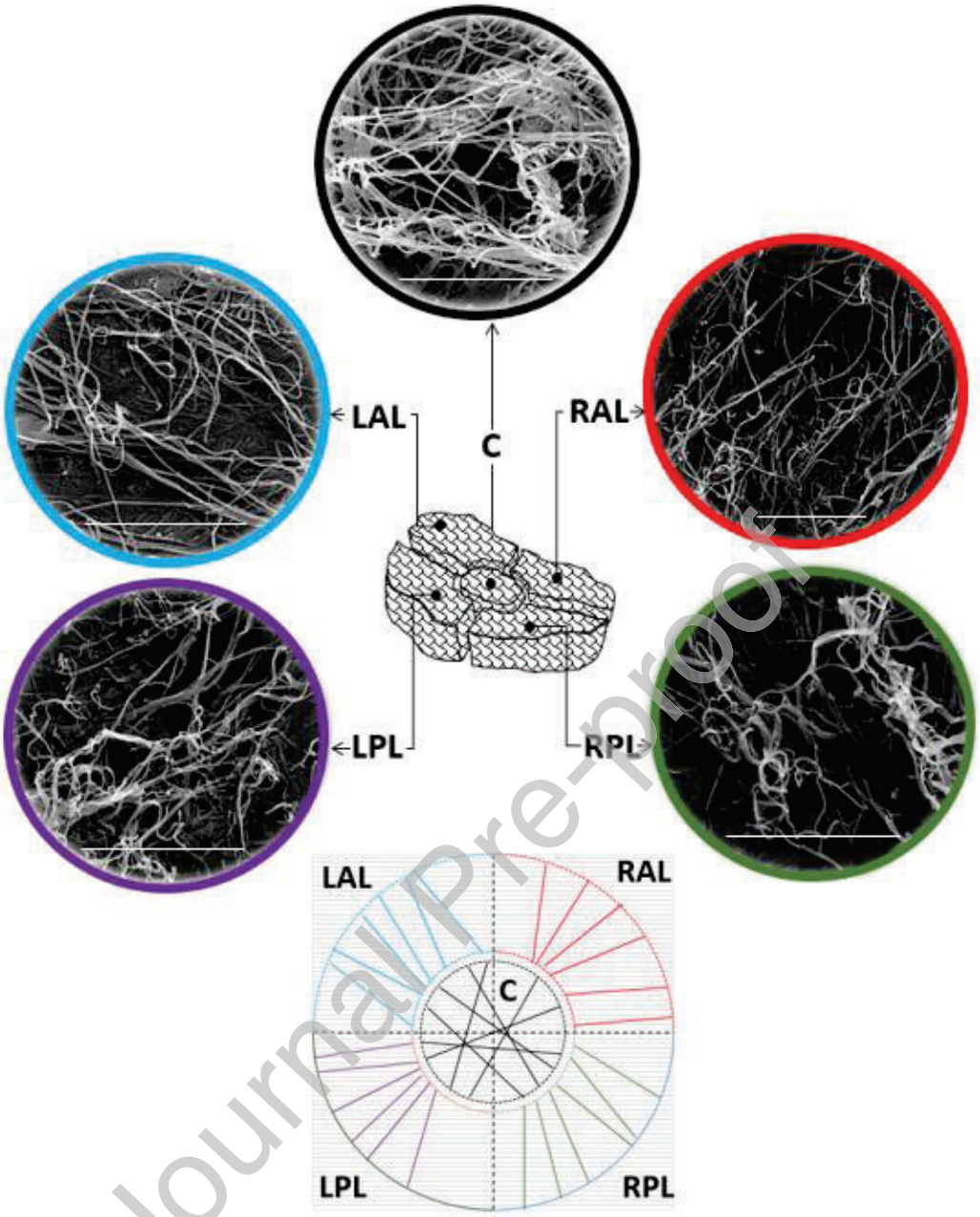

Figure 5- A schematic drawing representing the orientation of elastic fibers in different regions of the NP for all 6 samples (bottom) and SEM images (top) that were captured at similar magnifications from each region. Scale bars = 5 µm

Another interesting finding, not reported previously due to the lack of a reliable method for *in situ* isolation of elastic fibers, was the distribution of elastic fiber orientation in the NP (Figure 6).

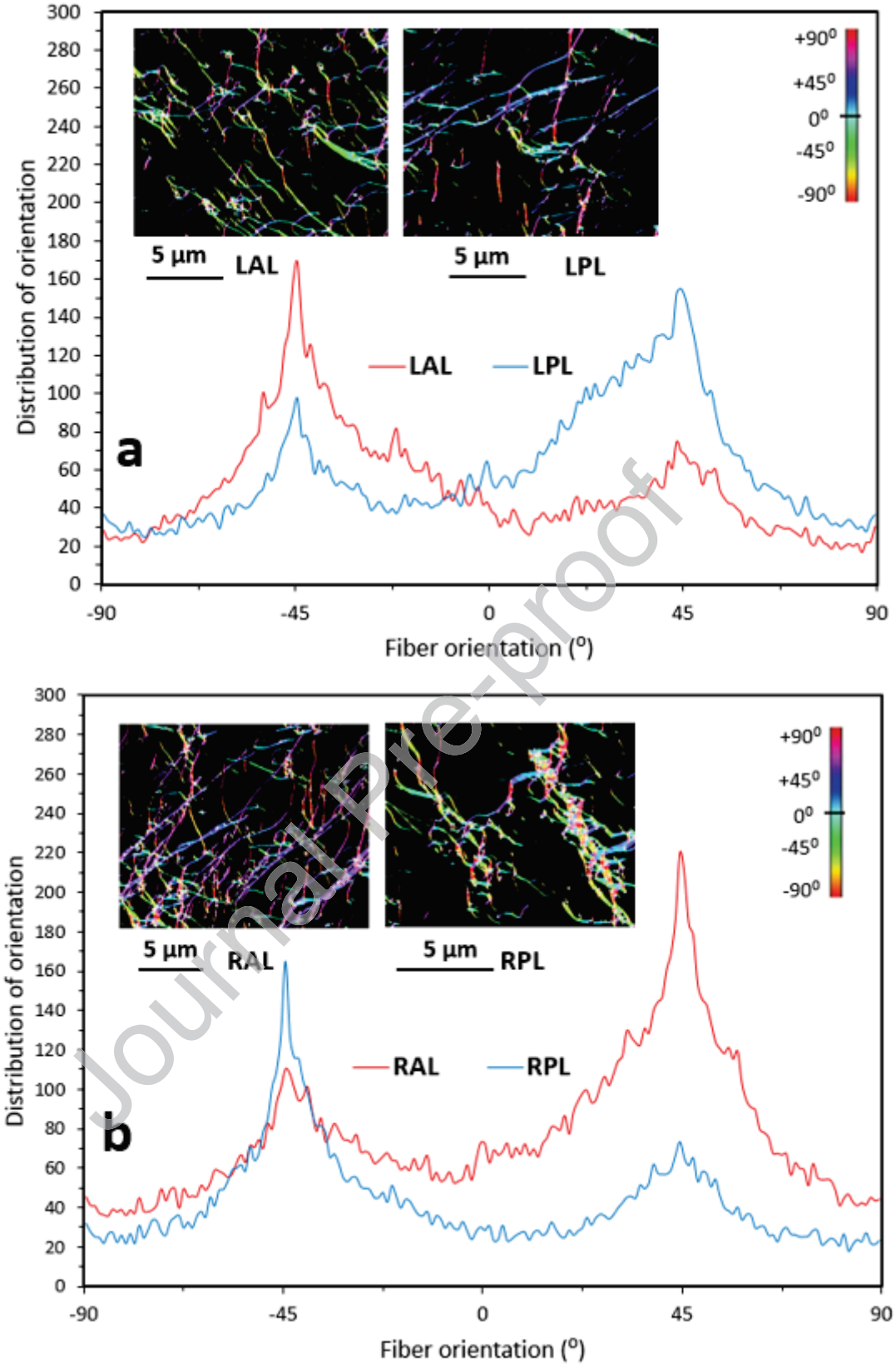

Figure 6- Distribution of elastic fiber orientation in different regions of the NP (AL: anterolateral; solid line and PL: posterolateral; dotted line) located in a) left (L) and b) right

(R) sides of the IVD. The orientation of fibers was measured relative to the lateral axis of the IVD, which was kept consistent among all samples during the experiments.

By analyzing the distribution of fiber orientation, one major organized angle of orientation (+45º or -45º) was detected in the anterior (red lines) and posterior (blue lines) regions of the NP (Figure 6a, 6b), with stronger peaks were observed for the anterior regions compared to the posterior regions. In addition, for the elastic fibers with an angle of orientation of +45º, a symmetrical peak with lower density was observed at -45º and vice versa. This observation indicated that the anterior region has a more dense elastic network organized at +45º or -45º, compared to the posterior region of the NP. We found that the distribution of elastic fibers in the central NP was different from those located at the peripheral regions with two symmetrically organized major peaks (±45º) of equal density observed (Figure 7).

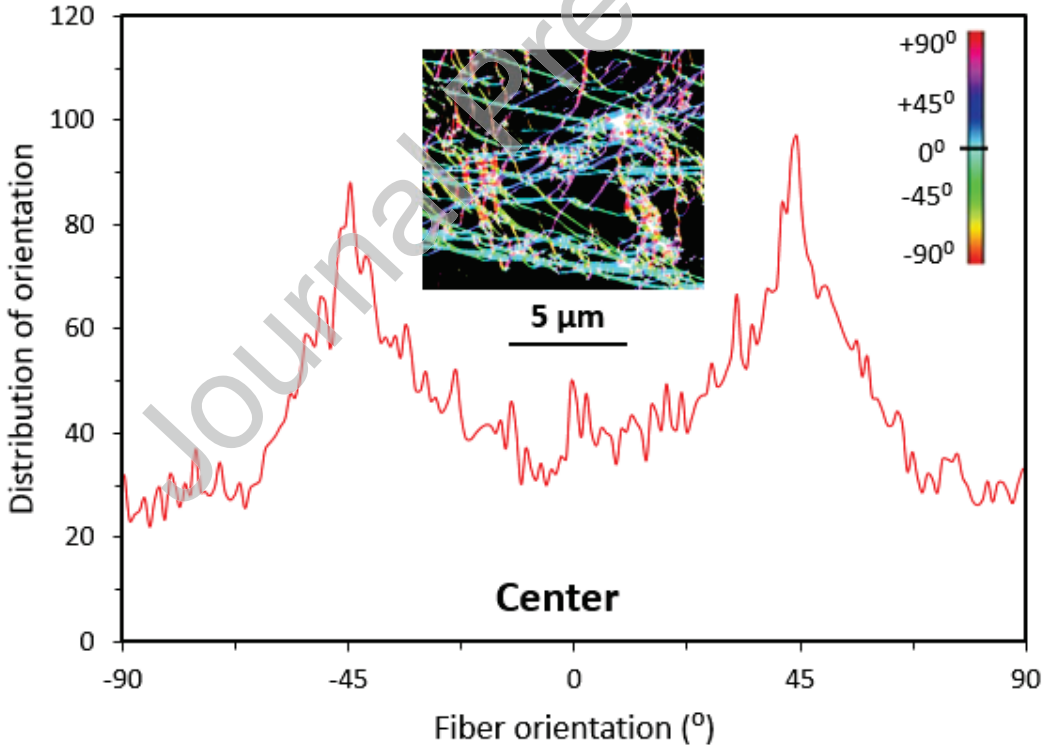

Figure 7 - Distribution of elastic fiber orientation in the central region of the NP. The orientation of fibers was measured relative to the lateral axis of the IVD, which was consistent among all samples during the experiment.

Similar numbers of fibers were measured in all regions of the NP ($p = 0.427$), based on quantitative analysis for measurement of the maximum fiber count at major angles of orientation (Supplementary S3). In addition, no significant difference was found for the maximum fiber counts occurring at major angles of orientation (±45º) for the central NP ($p = 0.788$).

The second aim of the current study was to present a structural model for the elastic fibers in the NP to ultimately contribute to the development of more reliable tissue-engineered scaffolds for NP regeneration. Based on SEM images that were captured after the elimination of all components, except for elastic fibers, a geometric representation of the elastic fiber network within the NP was obtained for the first time (Figure 8). The elastic fibers present a continuous network across the NP, comprising of thick and thin fibers. The thick elastic fibers are the major component in this network. They are long and mainly straight with an average thickness of 890 ± 12 nm and run from side to side of the NP at different angles of rotation (0º - 360º). The average distance between the thick fibers was measured as 13 ± 6 µm and 7± 2 µm at the peripheral and central regions of the NP, respectively. These major fibers are connected by thin fibers which are wavy in shape and can be divided into two different groups in terms of size, with average diameters of 215 ± 20 and 53 ±7 nm. The high-density nodes, produced by physical entanglement of thin fibers, were mainly located between the thick fibers and occupied an area of 5 × 5 μm^2, approximately.

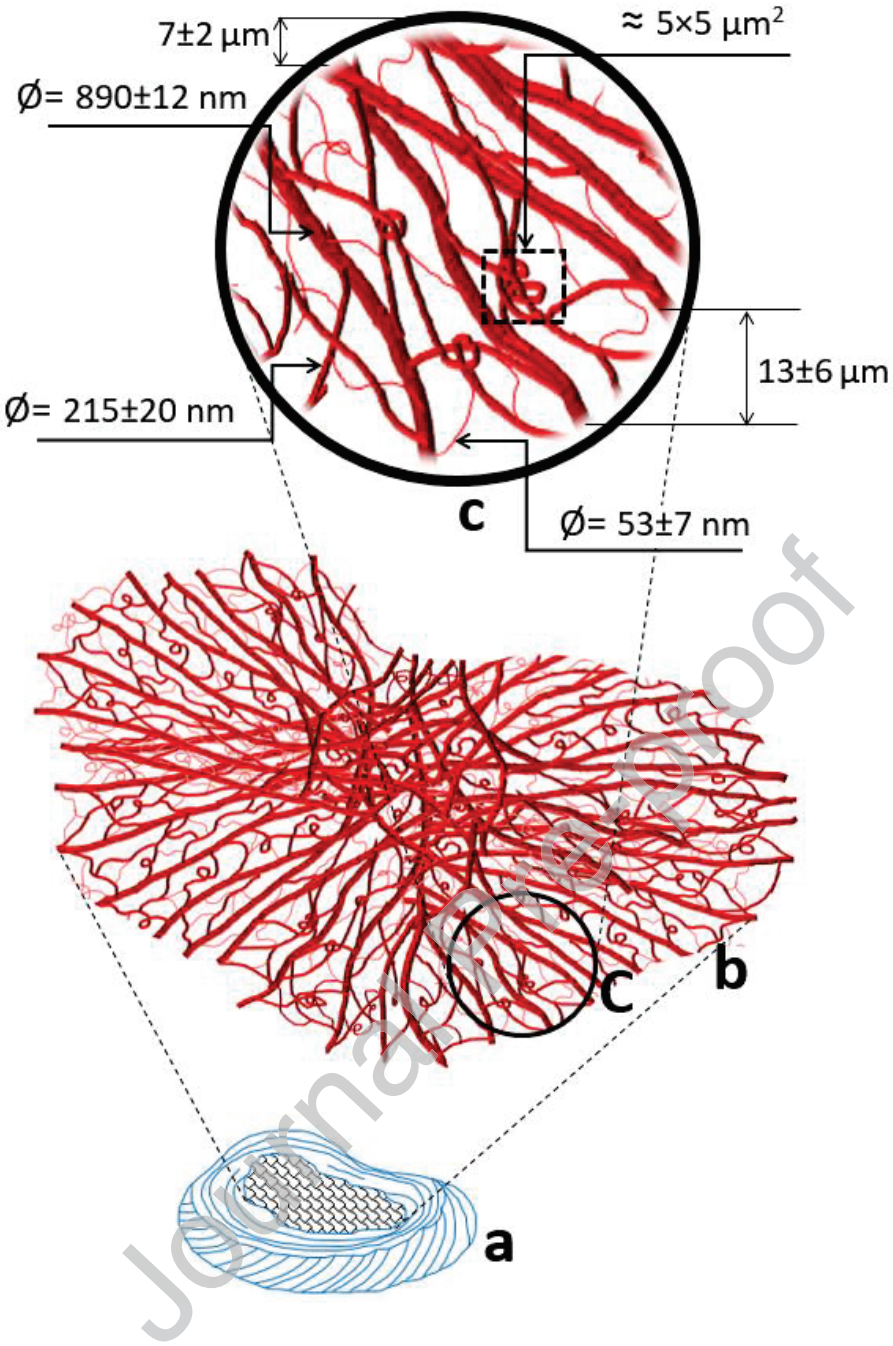

Figure 8- Schematic drawing of (a) an IVD including (b) the structural organization of elastic fibers across the NP to (c) present the geometrical analysis of elastic fibers network based on SEM images. The black circle denoted by "c" corresponds to the higher magnified image shown in "C". Since no significant differences for the thickness of the elastic fibers were observed across different regions of interest, the geometrical model is valid for the entire NP.

4. Discussion

The current study was designed to determine the ultrastructural organization of elastic fibers across the NP in sheep IVD and to develop a structural model for the elastic fibers in the NP using quantitative analysis. The presence of sparse elastic fibers in the NP of the IVD and their irregular distribution with radial orientation have been reported previously using conventional light microscope investigations [17-23]. However, previous qualitative explorations have neither revealed the fine-scale architectural details of the elastic fibers network nor have provided insight into their ultrastructural organization within the NP. While biological response of dics cells to mechanical stimuli are known [32, 33], the role of eastic fibers in delivering or altering those mechanical stimuli needs elucidation. This knowledge gap of the structure-function relationship of elastic fibers in the NP motivated the current study. Ultimately, Both qualitative and quantitative results presented for the ultrastructural organization of elastic fibers in the NP can be used for the fabrication of bio-inspired tissue-engineered IVD that truly replicates the multi-scale structural hierarchy of IVDs.

Since elastic fibers are intermingled with other fibrous components and are mostly obscured by the ECM, a previously developed digestion technique was employed to eliminate all components from the NP except for elastic fibers (Figure 2). Due to the heterogeneity of the NP composition, the digestion process removed the ECM to form separate regions revealing a fenestrated structure with the regions between fenestrations remaining approximately intact (partial digestion). As a consequence of partial digestion, a fenestration structure of small but various sizes was randomly scattered across the NP consisting of elastic fibers that were structurally supported by the undigested regions. While it was possible to carry on the process until full digestion of the samples, to completely isolate the elastic fibers, our approach to partially remove the extracellular matrix was critical to minimize structural alteration for further structural organization studies (Figure 3). Studies have shown that alkali

digestion resulted in isolation of elastin with intact inter-molecular cross-links and a surface appearance, without a coat of microfibrils, comparable to pure elastic fibers [34, 35]. Despite successful in situ isolation and visualization of elastic fibers network in the NP, appropriate optimization of the proposed methodology is crucial for tissues containing loose and spars hierarchical assembly of fibers or conditions such as age, degeneration, and disease affecting the density of elastic fibers [36]. While interests are growing to understand the biological and structural property of elastic fibers in such conditions, partial alkali digestion of the ECM may address the associated challenge.

The current study revealed for the first time, that elastic fibers form a network across the NP consisting of straight and thick parallel fibers that were interconnected by thin wavy fibers and ultrathin strands (Figures 3, 4 and Table 1). Apparently, in all regions of the NP except the central region, elastic fibers were extended from the center towards the AF with significant preferential orientation ($P < 0.001$), and therefore likely to provide a continuous elastic network across the IVD (Figure 5 and Table 2). The identification of the preferential orientation of elastic fibers helps compare ultrastructural organization of elastic fibers in healthy and mildly degenerated IVDs. This will likely immprove the understanding the role of elastic fibers play during overloading and progression to clinically relevant herniation [37]. In addition, the preferential orientation of elastic fibers in the IVD can elucidate the impact of ultrastructure on cell morphology and cellular orientation. Finally, the overall orientation of elastic fibers in the different regions of the IVD will be invaluable to build next generation of structural computational models and tissue-engineered constructs. The distribution of orientation for the elastic fibers in the NP occurred in one major organized angle of orientation (+45º or -45º) except for the central NP. We found that the distribution of elastic fibers in the central NP was different from those located in the peripheral regions, which was characterized by two symmetrically organized major peaks (±45º). Compared to two similar

studies that were performed in the AF of the IVD, it was found that the distribution of elastic fibers orientation in the NP was different from those located in the AF [26, 27]. Due to the lack of similar studies in the literature, it was difficult to compare the outcome of the current study with others. However, the findings here were consistent with light microscopic studies that reported the presence of long and radially orientated elastic fibers in the NP [19, 20].

The results of the current study identified that the interconnecting network of the elastic fibers in the NP was not randomly organized. Although not yet clear, this organization of the elastic fibers network in the NP suggests a mechanical role that may contribute to maintaining the NP structure [38]. Previous studies indicated that collagen fibers provide a significant connection between the NP and endplate and the NP transmits load equally to all parts of the AF [39-42]. This can be readily explained based on the results of the current study revealing a continuous elastic network consisting of long elastic fibers that running radially towards the AF. Overall, the elastic network in the NP is more likely to play a role in preserving the structural integrity of the NP through being stretched radially and contributes to its recovery after deformation. More importantly, the connectivity of elastic fibers with other extracellular matrix components through physical entanglement or chemical crosslinking may emphasize their mechanical role.

To date, the role of elastic fibers has been ignored in IVD models due to the absence of an appropriate methodology to visualize their ultrastructure *in situ*. The geometrical presentation, along with the distribution of elastic fibers, resulting from the present study identify the ultrastructural organization of elastic fibers in the NP which is important towards understanding their mechanical role which is still under investigation. Given the results of this new geometrical analysis, more-accurate multiscale finite element models can now be developed, which will provide new insights into the mechanobiology of the IVD. More importantly, limited tissue engineering approaches to construct tissue-engineered scaffolds,

have failed to capture the multi-scale structural hierarchy of discs due to the absence of an appropriate methodology to visualize their ultrastructure *in situ* [43-45]. It is important to note that the fabrication of structural models including synthetic elastic to replicate the property similar to the native tissue is challenging.

5. Conclusion

The current research is the first study to identify the ultrastructural organization of elastic fibers in the NP of the IVD that was performed using an innovative, easy and cost-effective methodology. We have found a well-organized network of thin and thick elastic fibers which appear to form a continuous network across the NP. Both qualitative and quantitative results presented for the ultrastructural organization of elastic fibers in the NP are crucial for a better understanding of their role in the structural integrity of the IVD. In addition, the results of this study can potentially be used for the fabrication of bio-inspired tissue-engineered scaffolds and IVD models to truly capture the multi-scale structural hierarchy of IVDs. To this end, the digestion technique developed here has been used successfully for in situ isolation of elastic fibers leading to the clarification of novel structural features for elastic fibers in the AF and NP regions of the IVD. Noting the different structural, material and biological properties between the AF and NP, the digestion technique is very likely to be employed for ultrastructural analysis of elastic fibers in different biological tissues to advance the scientific knowledge of the structure-property relationships in soft tissues. However, the limited visualization of elastic fibers in tissues containing loose and sparse hierarchical assemblies of fibers needs to be carefully considered.

Acknowledgments

Javad Tavakoli is grateful for the support of the University of Technology Sydney (UTS) with a Chancellor's Postdoctoral Research Fellowship (CPDRF) for the research work.

Conflict of interest

The authors declare no conflict of interest.

References

[1] J.J. Cassidy, A. Hiltner, E. Baer, Hierarchical structure of the intervertebral disc, Connect Tissue Res 23(1) (1989) 75-88.
[2] J. Raastad, M. Reiman, R. Coeytaux, L. Ledbetter, A.P. Goode, The association between lumbar spine radiographic features and low back pain: A systematic review and meta-analysis, Seminars in Arthritis and Rheumatism 44(5) (2015) 571-585.
[3] A.B. Sabnis, U. Chamoli, A.D. Diwan, Is L5–S1 motion segment different from the rest? A radiographic kinematic assessment of 72 patients with chronic low back pain, European Spine Journal 27(5) (2018) 1127-1135.
[4] S. Miyazaki, A.D. Diwan, K. Kato, K. Cheng, W.C. Bae, Y. Sun, J. Yamada, C. Muehleman, M.E. Lenz, N. Inoue, ISSLS PRIZE IN BASIC SCIENCE 2018: Growth differentiation factor-6 attenuated pro-inflammatory molecular changes in the rabbit anular-puncture model and degenerated disc-induced pain generation in the rat xenograft radiculopathy model, European Spine Journal 27(4) (2018) 739-751.
[5] R. Kandel, S. Roberts, J.P.G. Urban, Tissue engineering and the intervertebral disc: the challenges, European spine journal : official publication of the European Spine Society, the European Spinal Deformity Society, and the European Section of the Cervical Spine Research Society 17 Suppl 4(Suppl 4) (2008) 480-491.
[6] H.J. Wilke, P. Neef, M. Caimi, T. Hoogland, L.E. Claes, New in vivo measurements of pressures in the intervertebral disc in daily life, Spine (Phila Pa 1976) 24(8) (1999) 755-62.
[7] J. Yang, L. Wang, W. Zhang, Z. Sun, Y. Li, M. Yang, D. Zeng, B. Peng, W. Zheng, X. Jiang, G. Yang, Reverse Reconstruction and Bioprinting of Bacterial Cellulose-Based Functional Total Intervertebral Disc for Therapeutic Implantation, Small 14(7) (2018) 1702582.
[8] R. Kandel, S. Roberts, J.P. Urban, Tissue engineering and the intervertebral disc: the challenges, European Spine Journal 17(4) (2008) 480-491.
[9] M. D'Este, D. Eglin, M. Alini, Lessons to be learned and future directions for intervertebral disc biomaterials, Acta Biomaterialia 78 (2018) 13-22.
[10] X. Yang, X. Li, Nucleus pulposus tissue engineering: a brief review, Eur Spine J 18(11) (2009) 1564-72.
[11] S. van Uden, J. Silva-Correia, J.M. Oliveira, R.L. Reis, Current strategies for treatment of intervertebral disc degeneration: substitution and regeneration possibilities, Biomaterials Research 21(1) (2017) 22.
[12] P.J. Roughley, L.I. Melching, T.F. Heathfield, R.H. Pearce, J.S. Mort, The structure and degradation of aggrecan in human intervertebral disc, European Spine Journal 15(3) (2006) 326-332.
[13] G.Q. Teixeira, C. Leite Pereira, F. Castro, J.R. Ferreira, M. Gomez-Lazaro, P. Aguiar, M.A. Barbosa, C. Neidlinger-Wilke, R.M. Goncalves, Anti-inflammatory Chitosan/Poly-γ-glutamic acid nanoparticles control inflammation while remodeling extracellular matrix in degenerated intervertebral disc, Acta Biomaterialia 42 (2016) 168-179.
[14] C. Ligorio, M. Zhou, J.K. Wychowaniec, X. Zhu, C. Bartlam, A.F. Miller, A. Vijayaraghavan, J.A. Hoyland, A. Saiani, Graphene oxide containing self-assembling peptide hybrid hydrogels as a potential 3D injectable cell delivery platform for intervertebral disc repair applications, Acta Biomaterialia 92 (2019) 92-103.

[15] S.E. Gullbrand, D.H. Kim, E. Bonnevie, B.G. Ashinsky, L.J. Smith, D.M. Elliott, R.L. Mauck, H.E. Smith, Towards the scale up of tissue engineered intervertebral discs for clinical application, Acta Biomaterialia 70 (2018) 154-164.
[16] J.T. Martin, A.H. Milby, J.A. Chiaro, D.H. Kim, N.M. Hebela, L.J. Smith, D.M. Elliott, R.L. Mauck, Translation of an engineered nanofibrous disc-like angle-ply structure for intervertebral disc replacement in a small animal model, Acta Biomaterialia 10(6) (2014) 2473-2481.
[17] J. Yu, P.C. Winlove, S. Roberts, J.P.G. Urban, Elastic fibre organization in the intervertebral discs of the bovine tail, J Anat 201(6) (2002) 465-475.
[18] E.F. Johnson, H. Berryman, R. Mitchell, W.B. Wood, Elastic fibres in the anulus fibrosus of the adult human lumbar intervertebral disc. A preliminary report, J Anat 143 (1985) 57-63.
[19] L.J. Smith, N.L. Fazzalari, Regional variations in the density and arrangement of elastic fibres in the anulus fibrosus of the human lumbar disc, J Anat 209(3) (2006) 359-367.
[20] L.J. Smith, N.L. Fazzalari, The elastic fibre network of the human lumbar anulus fibrosus: architecture, mechanical function and potential role in the progression of intervertebral disc degeneration, European Spine Journal 18(4) (2009) 439-448.
[21] J. Buckwalter, R. Cooper, J. Maynard, Elastic fibers in human intervertebral discs, JBJS 58(1) (1976) 73-76.
[22] J. Yu, U. Tirlapur, J. Fairbank, P. Handford, S. Roberts, C. Winlove, Z. Cui, J. Urban, Microfibrils, elastin fibres and collagen fibres in the human intervertebral disc and bovine tail disc, J Anat 210 (2007) 460-71.
[23] B. Johnstone, M. Markopoulos, P. Neame, B. Caterson, Identification and characterization of glycanated and non-glycanated forms of biglycan and decorin in the human intervertebral disc, Biochem J 292 (Pt 3) (1993) 661-6.
[24] J. Tavakoli, J.J. Costi, Development of a rapid matrix digestion technique for ultrastructural analysis of elastic fibers in the intervertebral disc, Journal of the mechanical behavior of biomedical materials 71 (2017) 175-183.
[25] J. Tavakoli, J.J. Costi, A method for visualization and isolation of elastic fibres in annulus fibrosus of the disc, Materials Science and Engineering: C 93 (2018) 299-304.
[26] J. Tavakoli, D.M. Elliott, J.J. Costi, The ultra-structural organization of the elastic network in the intra- and inter-lamellar matrix of the intervertebral disc, Acta Biomaterialia 58 (2017) 269-277.
[27] J. Tavakoli, J.J. Costi, Ultrastructural organization of elastic fibres in the partition boundaries of the annulus fibrosus within the intervertebral disc, Acta Biomaterialia 68 (2018) 67-77.
[28] J. Tavakoli, J.J. Costi, New findings confirm the viscoelastic behaviour of the inter-lamellar matrix of the disc annulus fibrosus in radial and circumferential directions of loading, Acta Biomaterialia 71 (2018) 411-419.
[29] J. Tavakoli, J.J. Costi, New insights into the viscoelastic and failure mechanical properties of the elastic fiber network of the inter-lamellar matrix in the annulus fibrosus of the disc, Acta Biomaterialia 77 (2018) 292-300.
[30] J. Tavakoli, D.M. Elliott, J.J. Costi, Structure and mechanical function of the inter-lamellar matrix of the annulus fibrosus in the disc, Journal of Orthopaedic Research 34(8) (2016) 1307-1315.
[31] H. Inoue, T. Takeda, Three-dimensional observation of collagen framework of lumbar intervertebral discs, Acta Orthop Scand 46(6) (1975) 949-56.
[32] A.H. Hsieh, J.D. Twomey, Cellular mechanobiology of the intervertebral disc: new directions and approaches, Journal of biomechanics 43(1) (2010) 137-145.
[33] J.J. MacLean, C.R. Lee, M. Alini, J.C. Iatridis, The effects of short-term load duration on anabolic and catabolic gene expression in the rat tail intervertebral disc, Journal of Orthopaedic Research 23(5) (2005) 1120-1127.
[34] F. Steven, R. Minns, H. Thomas, The isolation of chemically pure elastins in a form suitable for mechanical testing, Connective tissue research 2(2) (1974) 85-90.
[35] T. Ushiki, Collagen fibers, reticular fibers and elastic fibers. A comprehensive understanding from a morphological viewpoint, Archives of histology and cytology 65(2) (2002) 109-126.

[36] H. Tseng, K.J. Grande-Allen, Elastic fibers in the aortic valve spongiosa: a fresh perspective on its structure and role in overall tissue function, Acta biomaterialia 7(5) (2011) 2101-2108.
[37] J. Tavakoli, D.B. Amin, B.J. Freeman, J.J. Costi, The biomechanics of the inter-lamellar matrix and the lamellae during progression to lumbar disc herniation: which is the weakest structure?, Annals of biomedical engineering 46(9) (2018) 1280-1291.
[38] C.M. Disney, A. Eckersley, J.C. McConnell, H. Geng, A.J. Bodey, J.A. Hoyland, P.D. Lee, M.J. Sherratt, B.K. Bay, Synchrotron tomography of intervertebral disc deformation quantified by digital volume correlation reveals microstructural influence on strain patterns, Acta Biomaterialia 92 (2019) 290-304.
[39] A. Nachemson, Lumbar intradiscal pressure. Experimental studies on post-mortem material, Acta Orthop Scand Suppl 43 (1960) 1-104.
[40] J.C. Iatridis, M. Weidenbaum, L.A. Setton, V.C. Mow, Is the Nucleus Pulposus a Solid or a Fluid? Mechanical Behaviors of the Nucleus Pulposus of the Human Intervertebral Disc, Spine 21(10) (1996) 1174-1184.
[41] J.C. Iatridis, L.A. Setton, M. Weidenbaum, V.C. Mow, Alterations in the mechanical behavior of the human lumbar nucleus pulposus with degeneration and aging, Journal of Orthopaedic Research 15(2) (1997) 318-322.
[42] K.R. Wade, P.A. Robertson, N.D. Broom, A fresh look at the nucleus-endplate region: new evidence for significant structural integration, European Spine Journal 20(8) (2011) 1225-1232.
[43] Y.-C. Chen, W.-Y. Su, S.-H. Yang, A. Gefen, F.-H. Lin, In situ forming hydrogels composed of oxidized high molecular weight hyaluronic acid and gelatin for nucleus pulposus regeneration, Acta Biomaterialia 9(2) (2013) 5181-5193.
[44] A.C. Borges, C. Eyholzer, F. Duc, P.-E. Bourban, P. Tingaut, T. Zimmermann, D.P. Pioletti, J.-A.E. Månson, Nanofibrillated cellulose composite hydrogel for the replacement of the nucleus pulposus, Acta Biomaterialia 7(9) (2011) 3412-3421.
[45] A.T. Reza, S.B. Nicoll, Characterization of novel photocrosslinked carboxymethylcellulose hydrogels for encapsulation of nucleus pulposus cells, Acta Biomaterialia 6(1) (2010) 179-186.

Graphical abstract